Available online at www.sciencedirect.com
SCIENCE DIRECT®
Coordination Chemistry Reviews 249 (2005) 1653–1663
COORDINATION CHEMISTRY REVIEWS
www.elsevier.com/locate/ccr

Review

Iron hydrogenase active site mimics in supramolecular systems aiming for light-driven hydrogen production

Licheng Sun [a,**], Björn Åkermark [a], Sascha Ott [b,*]

[a] *Department of Organic Chemistry, Arrhenius Laboratory, Stockholm University, Stockholm, Sweden*
[b] *Department of Organic Chemistry, BMC, Uppsala University, Box 599, 75123 Uppsala, Sweden*

Received 30 June 2004; accepted 23 January 2005
Available online 5 March 2005

Contents

Abstract

Models of the iron hydrogenase active site [(μ-DT)$Fe_2(CO)_6$] (DT: dithiolate) have been synthesized where the dithiolate co-factor bears a functional group to allow for their incorporation into supramolecular systems. Covalently linked to ruthenium(II) polypyridyl photosensitizers, the resulting ruthenium–diiron complexes represent the first members of a new class of dyads designed to promote the light-driven production of hydrogen. The functionalized diiron complexes have been characterized by X-ray crystallography. The redox properties of all complexes were investigated by cyclic voltammetry and the interactions between the photo-excited ruthenium moiety and the diiron unit in these dyads were evaluated by time-resolved spectroscopy.

Keywords: Bioinorganic chemistry; Electron transfer; Enzyme models; Iron hydrogenase; Ruthenium

* Corresponding author. Tel.: +46 184714825; fax: +46 184713818.
** Co-corresponding author. Present address: KTH Chemistry, Organic Chemistry, Royal Institute of Technology, Stockholm, Sweden.
E-mail addresses: lichengs@kth.se (L. Sun), bjorn.akermark@organ.su.se (B. Åkermark), sascha.ott@fki.uu.se (S. Ott).

0010-8545/$ – see front matter © 2005 Elsevier B.V. All rights reserved.
doi:10.1016/j.ccr.2005.01.013

1. Light-driven hydrogen production

1.1. Background

Efforts to harness renewable energies since the 1970s have mainly been driven by concerns about the "energy security", that is the fear about the limited availability of fossil fuels in the future [1]. The access to fossil fuels has become a complex political issue which imposes great threats to the political stability of nations in the Middle East and other regions on the planet. The growing population together with the industrial development on the Asian continent has intensified these problems further [2]. In the last decade, environmental concerns have provided additional motivation for scientists to move the world forward towards renewable, alternative forms of energy. Carbon dioxide has been identified as the main agent responsible for green house effect and global warming and large efforts are considered to be necessary in order to achieve a stabilisation of the atmospheric carbon dioxide content [3,4]. The capture of sunlight and its conversion into readily available forms of energy may be able to satisfy mankind's energy demands of the future. Unless used directly for solar heating, sunlight is usually converted to electricity, a form of energy which is difficult to store and is best consumed the instant it is produced. Conversion of solar energy into hydrogen, on the other hand, provides a solution to this problem, as hydrogen is a valuable fuel which can be stored in large quantities in pressurized vessels. With the development of more efficient fuel cells, molecular hydrogen has now emerged as a true alternative to fossil fuels as the energy carrier of the future [5]. From an environmental viewpoint, combustion of hydrogen is unobjectionable since the only "waste" product is water (Eq. (1)).

$$2H_2 + O_2 \rightleftharpoons 2H_2O \quad (1)$$

Until now, the production of hydrogen has relied mainly on fossil fuels, a fact which makes the idea of its use as a clean fuel highly debatable. If the reverse reaction of Eq. (1), that is the splitting of water, could be driven directly by the action of light, hydrogen could be produced and combusted in a truly cyclic process with no waste product ever being formed. This perspective provides the motivation for the development of supramolecular systems capable of catalyzing the light-driven splitting of water.

One of the main difficulties in achieving the splitting of water by light-induced charge transfer events is that the two half reactions are multi-electron processes. The generation of hydrogen (Eq. (2)) requires two and the oxidation of water (Eq. (3)) releases four electrons [6].

$$2H_2O + 2e^- \rightarrow H_2 + 2OH^- \quad (2)$$

$$2H_2O \rightarrow O_2 + 4H^+ + 4e^- \quad (3)$$

With the standard potential for Eq. (2) being −0.41 V versus normal hydrogen electrode (NHE) and that for Eq. (3) being +0.81 V at pH 7, photons with an energy higher than 1.23 eV, which corresponds to minimum energy of 1008 nm could theoretically induce the cleavage of water. The absence of any water absorption in the visible region together with the fact that the cleavage reaction involves multi-electron transfer processes is responsible for large overpotentials and that his photoreaction does not occur under ambient conditions.

A supramolecular system designed for the oxidation/reduction of water has to contain certain elements which take both of these factors into account. A photosensitizer is required to harvest the incoming light and to transfer the reduction/oxidation equivalent to a suitable catalyst, which has to be capable to store two electrons for the reduction and four electron holes for the oxidation reaction. A molecular assembly that catalyzes both half reactions is unprecedented, however, model systems that address either half reaction have been described [6,7]. It is noteworthy that more systems for the two-electron reduction of water are known compared to the four electron oxidation. Some of these reports will briefly be discussed in the next section to illustrate the general principle of this process.

1.2. General principle and model systems

First reports of multi-component systems which were capable to catalyze the light-driven reduction of water appeared in the late 1970s, only a few years after the energy crisis. In perhaps the most prominent examples $[Ru(bpy)_3]^{2+}$ is employed as the photosensitizer [8–10]. Once excited by the absorption of a photon, $^*[Ru(bpy)_3]^{2+}$ is capable of reducing methyl viologen (Eq. (4)). The reduced methyl viologen radical cation can now react with water on the surface of a platinum dioxide catalyst to form hydrogen and thereby regenerate its dicationic form (Eq. (5)). The catalytic cycle is closed and the photosensitizer regenerated after reduction of the photo-oxidized ruthenium complex by triethanol amine (TEOA), which acts as a sacrificial electron donor (Eq. (6)).

$$^*[Ru(bpy)_3]^{2+} + MV^{2+} \rightarrow [Ru(bpy)_3]^{3+} + MV^{\bullet +} \quad (4)$$

$$2MV^{\bullet +} + 2H_2O \xrightarrow{PtO_2} 2MV^{2+} + H_2 + 2OH^- \quad (5)$$

$$TEOA + [Ru(bpy)_3]^{3+} \rightarrow TEOA^+ + [Ru(bpy)_3]^{2+} \quad (6)$$

Since these early reports, a variety of multi-component arrays have been examined for the reduction of water [6,7]. Polypyridyl complexes of ruthenium(II) or porphyrinoids are frequently employed as photosensitizers. Bipyridines, lanthanoid ions or transition metal complexes are used as electron mediators, amines and methoxybenzenes as sacrificial donors and noble metal complexes as proton reduction catalysts. More recently, heterogenous systems based on doped

TiO_2 semiconductors have attracted a lot of attention in this field [11,12].

2. Iron hydrogenase active site mimics

2.1. Model complexes and reactivity

Hydrogenases are enzymes which regulate the metabolism of hydrogen in cyanobacteria and other microorganisms. Having this function, they can catalyze both, the oxidation of hydrogen as well as the reduction of protons [13–15]. Iron hydrogenases seem to be more involved in the latter process and generally achieve higher turnover numbers than the evolutionary unrelated, but functionally related nickel–iron hydrogenases [16]. The structure determination of iron hydrogenases by X-ray crystallography has provided the synthetic chemist with crucial information of the composition of its active site (Chart 1a) [17,18]. In the so-called H-cluster, two iron cations are linked by an unusual bridging dithiolate ligand. This ligand has been suggested to contain a nitrogen hetero-atom and to possess the structure S–CH_2–NH–CH_2–S [19,20]. The remaining primary coordination sphere around the dinuclear iron core is occupied by CO and CN^- diatomic ligands as well as by a thiol-linked tetranuclear iron cluster which is part of the electron transfer chain to and from the active site [13,14]. In the natural system one coordination site remains vacant to allow for hydride, water or hydrogen coordination.

Fuelled by this knowledge, great efforts have been directed towards the preparation of model complexes mimicking the structure as well as the function of the natural system. The "parent" propyldithiolate (PDT)-bridged [(μ-PDT)$Fe_2(CO)_6$] **1** (Chart 1b) [21] has been synthesized and elaborated complexes have been prepared where carbonyl ligands were replaced by isonitriles [22], cyanides [23,24], thioethers [25–27] and phosphines [28,29]. Darensbourg and co-workers [28] have reported that [(μ-H)(μ-PDT)$Fe_2(CO)_4(PMe_3)_2]^+$ is a catalyst for H_2/D_2 scrambling, whereas Rauchfuss and co-workers [30,31] demonstrated that [(μ-PDT)$Fe_2(CO)_4PMe_3(CN)]^-$ serves as a catalyst for electrochemical hydrogen evolution. Ourselves, we have reported of [(μ-SCH_2-NHR-CH_2-S)$Fe_2(CO)_6]^+$ which catalyzes the electrochemical reduction of protons at the moderately negative potential of −1.4 V versus $Fc^{+/0}$ [32].

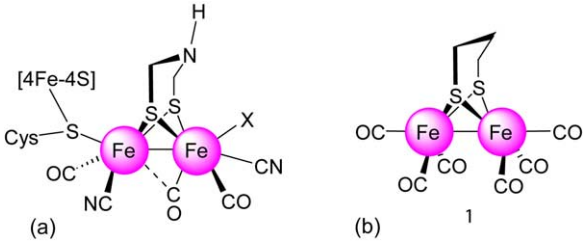

Chart 1.

2.2. Iron hydrogenase mimics in supramolecular systems—the hypothesis

In context of our interest in photochemical fuel production [33,34] we became intrigued by the possibility to covalently link a biomimetic model of the iron hydrogenase active site to a ruthenium photosensitizer in an attempt to afford hydrogen production by light. The projected process is illustrated in Fig. 1. It commences with the absorption of a photon by the ruthenium photosensitizer (step 1). The photo-excited ruthenium complex is oxidatively quenched by the dinuclear iron site, giving rise to a reduced iron species (step 2). After regeneration of the photosensitizer (by an external electron donor), this process is repeated in order to accumulate two electrons on the diiron unit. Alternatively, electron injection to the diiron site may be feasible from a ruthenium(I) complex which can be formed by reductive quenching of the ruthenium(II) excited state. Having acquired sufficient reducing power, the diiron complex should then be capable of reducing two protons and, hence, to generate hydrogen.

Naturally, the driving force for a second electron transfer to an already reduced diiron complex will be greatly diminished. However, we hope to be able to compensate for this effect by a protonation of the mono-reduced diiron species and hence, the neutralization of the generated charge. The possibility of introducing ligands different from CO on the diiron portion offers additional opportunities to alter the redox characteristics of the complex. With these options, we intend to tune the redox properties of the isolated components in the supramolecular structure to suit the electronic requirements for hydrogen evolution.

2.3. Functionalized diiron complexes

For the construction of ruthenium–diiron dyads, iron hydrogenase active site model complexes had to be designed which feature functional groups on the periphery of the diiron core to allow for the attachment of the photosensitizer. We identified the dithiolate bridge as the most suitable position for this chemistry and endeavoured in the synthesis of functionalized complexes. In the first instance, a complex with a free amine group was targeted as it would allow the attachment of the photosensitizer via an easily formed amide bond (Scheme 1) [35].

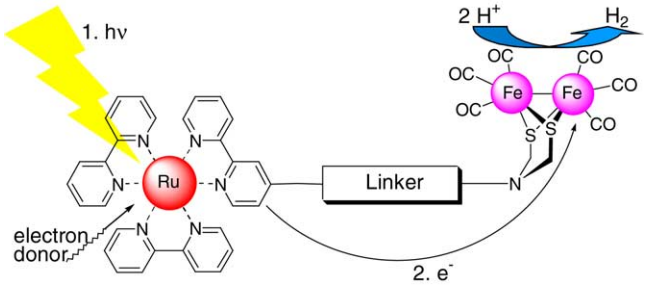

Fig. 1. Schematic representation of light-driven proton reduction.

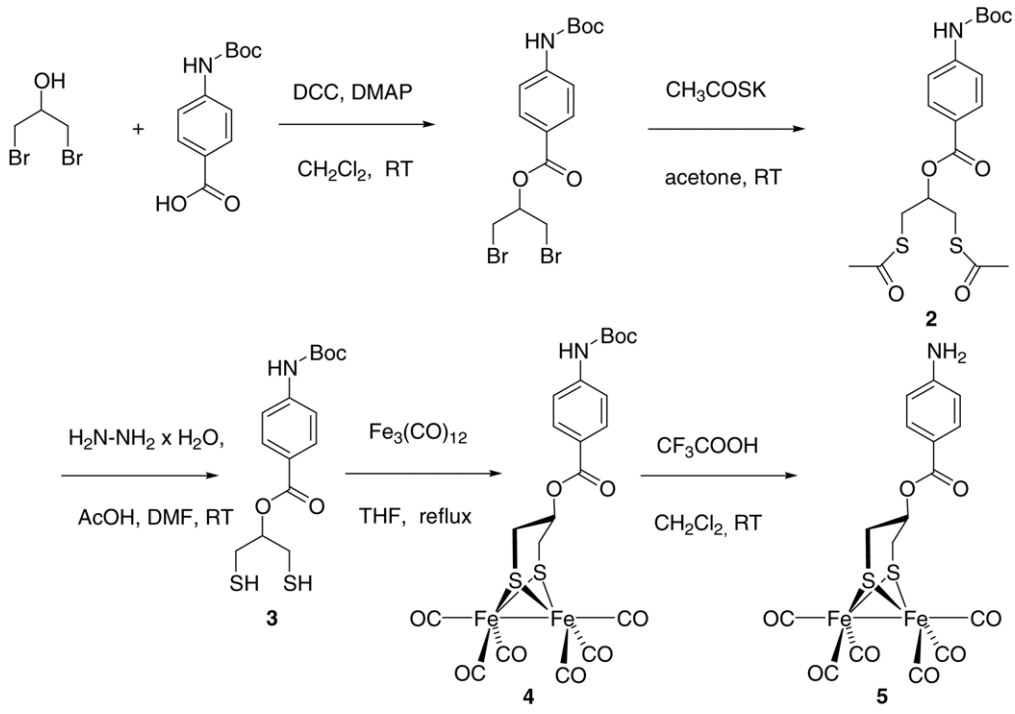

Scheme 1. Synthesis of amino-functionalised [(PDT)$Fe_2(CO)_6$] **5**.

The alcohol in 1,3-dibromopropan-2-ol was esterified with Boc-protected *p*-aminobenzoic acid under usual coupling conditions. Subsequent treatment with potassium thioacetate afforded the dithioacetate **2** which could be converted to the dithiol **3** by treatment with hydrazine monohydrate. Attachment of the diironhexacarbonyl moiety was afforded in the usual manner and the amine functionality was liberated under acidic conditions with TFA to form **5**.

Another diiron hexacarbonyl complex has recently been made available where the two iron nuclei are coordinated by cysteinyl ligands [36]. As illustrated in Scheme 2, complex **6** is accessible as a mixture of e,e and e,a isomers by an oxidative addition of cysteine to [$Fe_3(CO)_{12}$]. Interestingly, upon extended heating or addition of acetic acid to a solution of the complex in toluene, **6** undergoes an unusual intramolecular nucleophilic cyclization with inversion of the configuration to form the chiral ethyldithiolate-bridged diiron complex **7**. The molecular integrity of **7** and the absolute configuration of the chiral center was confirmed by single crystal X-ray diffraction analysis (Fig. 2).

Other approaches to synthesize functionalized active site models in our group are based on azadithiolate (ADT)-bridged systems and the idea that arylhalides can be bound to the nitrogen heteroatom. Moreover, this strategy benefits from the fact that the nitrogen heteroatom on the disulfide bridge offers a basic site close to the catalytic center, which is thought to be a crucial structural feature for the production of hydrogen in the enzyme [19,20]. The attach-

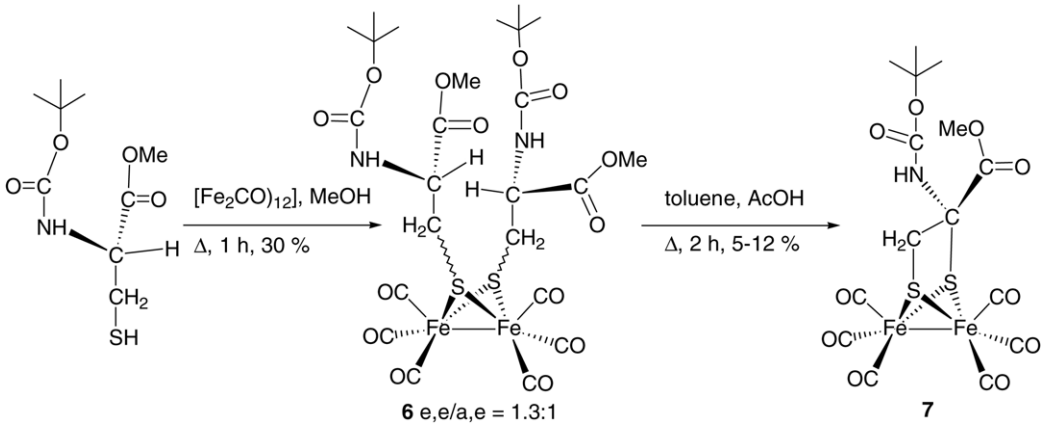

Scheme 2. Synthesis cysteine-ligated diiron complex **6** and its intramolecular cyclisation to **7**.

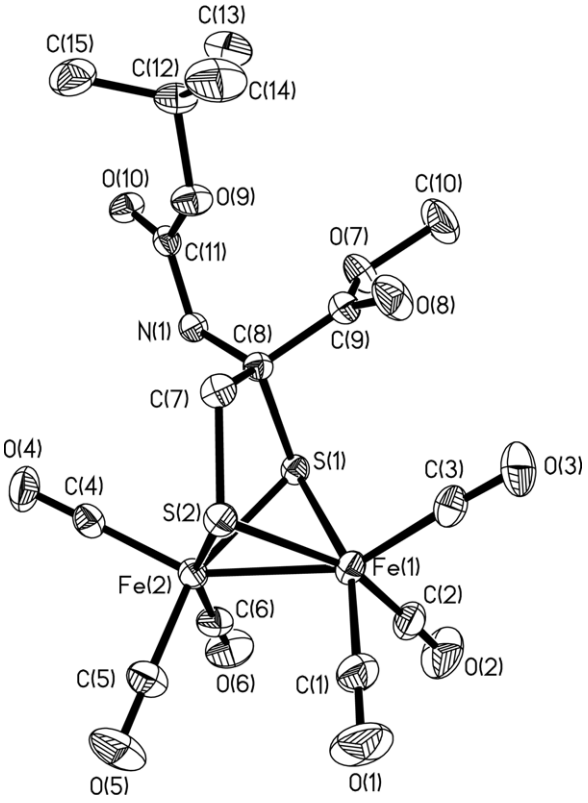

Fig. 2. ORTEP (ellipsoids at 30% probability level) view of **7**. Reproduced with permission of the copyright holders from [36].

ment of aryliodides or bromides allows the elaboration to supramolecular systems in palladium-mediated Sonogashira cross coupling reactions with suitable acetylenic photosensitizers [37]. Hence, 4-iodoaniline was reacted with the lithium salt of diironhexacarbonyl disulfide in THF at low temperature to afford the functionalized diiron complexes **8** in a single operation in good yield (Scheme 3) [37,38].

Complex **9** which features an additional methylene group between the nitrogen heteroatom in the dithiolate bridge and the aromatic moiety was synthesized from *p*-bromobenzylamine in a similar procedure [32].

The crystal structures of complexes **5**, **8** and **9** (Fig. 3) feature the usual pseudo square-pyramidal geometry around the iron nuclei where the two μ-S atoms, C1 and C2 define the base and C3 the apical position. The two iron nuclei are in bonding distance of 2.499(1), 2.499(1) and 2.5083(7) Å, respectively, in good agreement with the values reported for related structures [28,39]. As expected, the aromatic linker in **5** prefers an equatorial position of the metalloheterocycle. A similar solid state conformation is observed for the ADT-bridged complex **9**, where the organic tether is pointing away from the diiron core. In contrast to these conformations, the π-conjugation between the nitrogen heteroatom and the aromatic moiety in **8** forces the linker in a pseudo-axial position. As a consequence, the Fe–C–O angle between the nearby apical carbonyl ligand and the appended iron atom is considerably bent and has to adopt an angle of 173° compared to an almost linear geometry in **9**. This steric congestion is also reflected by the non-bonding C · · · N distance between the ADT nitrogen and the apical carbonyl carbon in **8**, which is significantly elongated compared to that in the benzyl-substituted analogue **9** (3.5 Å versus 3.02 Å).

As evident from the crystal structures, complexes **5**, **8** and **9** differ only marginally around the $Fe_2(CO)_6$ core, but significantly in the organic dithiolate ligand and the nature of its central atom. Spectroscopic and electrochemical measurements were conducted in order to probe the influence of this variation. The IR spectra of the complexes feature three signals in the carbonyl region between 2075 and 2000 cm^{-1}. A small difference is noticeable when comparing the PDT- and ADT-based complexes with the signals of the latter being shifted by 3–4 cm^{-1} towards higher wavenumbers.

The UV–vis spectra of the dinuclear iron complexes **5**, **8** and **9** are dominated by a strong absorption in the UV region around 270 nm. A second intense absorption is visible in the near UV around 330 nm. Depending on the coordination sphere around the iron nuclei, this absorption can be substantially shifted. This might be an indication for the involvement of metal as well as ligand orbitals in this transition. A broad and featureless absorption reaching up to 600 nm with an extinction coefficient of maximal 1800 M^{-1} cm^{-1} is responsible for the dark red colour of these iron coordination compounds. Albeit being only of relatively small amplitude, this absorption may become problematic since ruthenium polypyridyl complex are emitting in the same region.

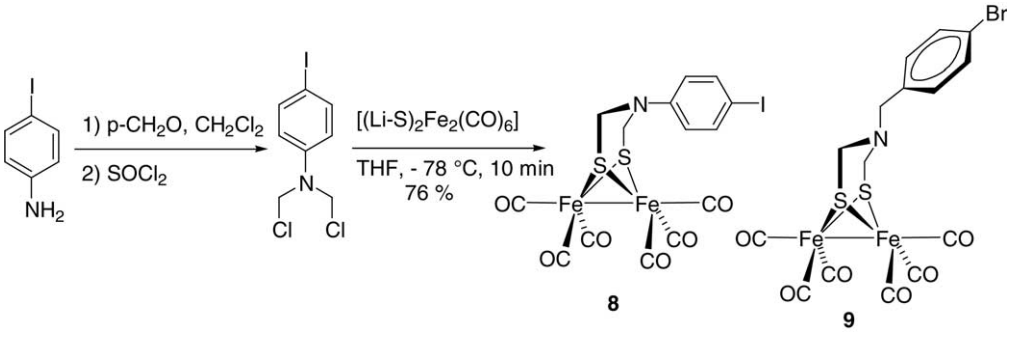

Scheme 3. Synthesis of functionalised, azadithiolate (ADT)-bridged diiron complexes **8**, **9**.

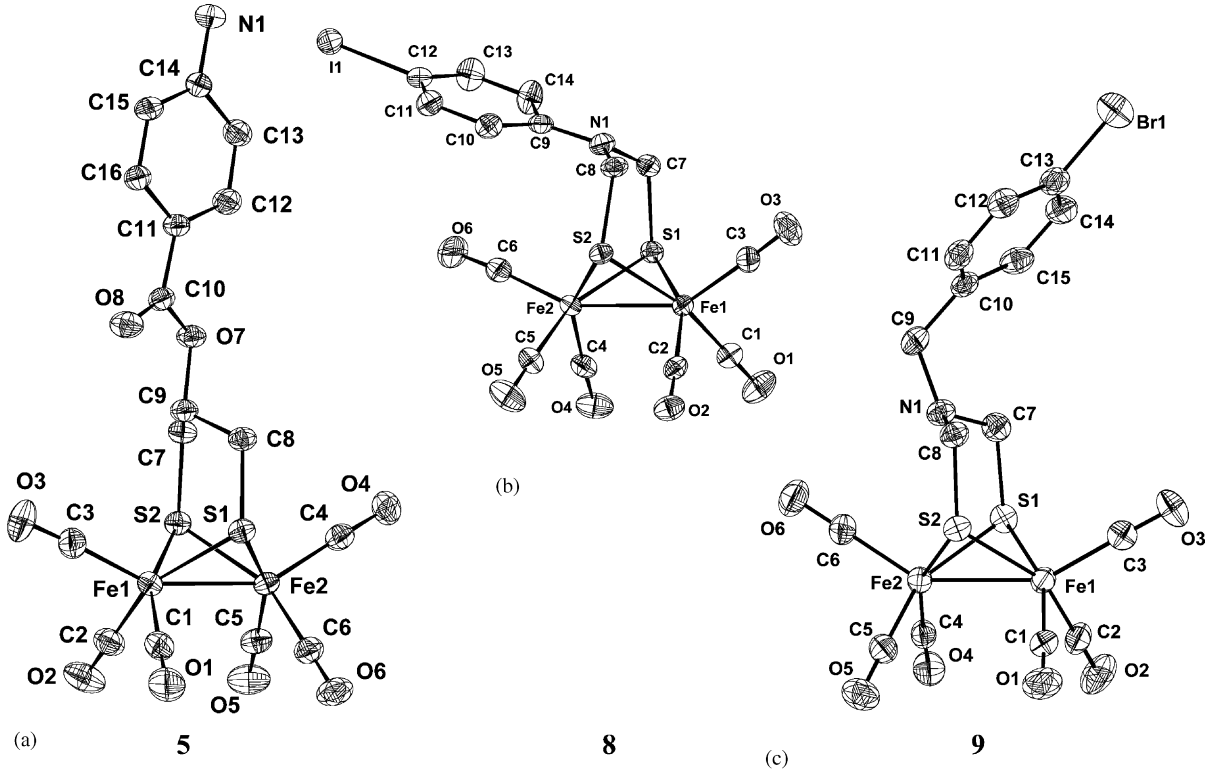

Fig. 3. ORTEP (ellipsoids at 30 % probability level) view of diiron hexacarbonyl complexes bearing functional groups: (a) **5**; (b) **8**; and (c) **9**.

As a result of the spectral overlap, the excited state of the ruthenium complex may be quenched by unwanted energy transfer processes to the diiron moiety.

The cyclic voltammogram of the diiron complex **4** features two irreversible oxidations below 1.0 V originating from an oxidation of the diiron moiety and of the amine functionality. On the cathodic scan, an irreversible reduction is observed at a potential typical for $[(\mu\text{-PDT})Fe_2(CO)_6]$ type of complexes at -1.69 V versus $Fc^{+/0}$ [40]. For the $[(\mu\text{-ADT})Fe_2(CO)_6]$ complexes **8** and **9**, an irreversible oxidation is observed at a potential around 0.60 ± 0.05 V versus $Fc^{+/0}$. The exact location of this process is ambiguous as it could be centred on the

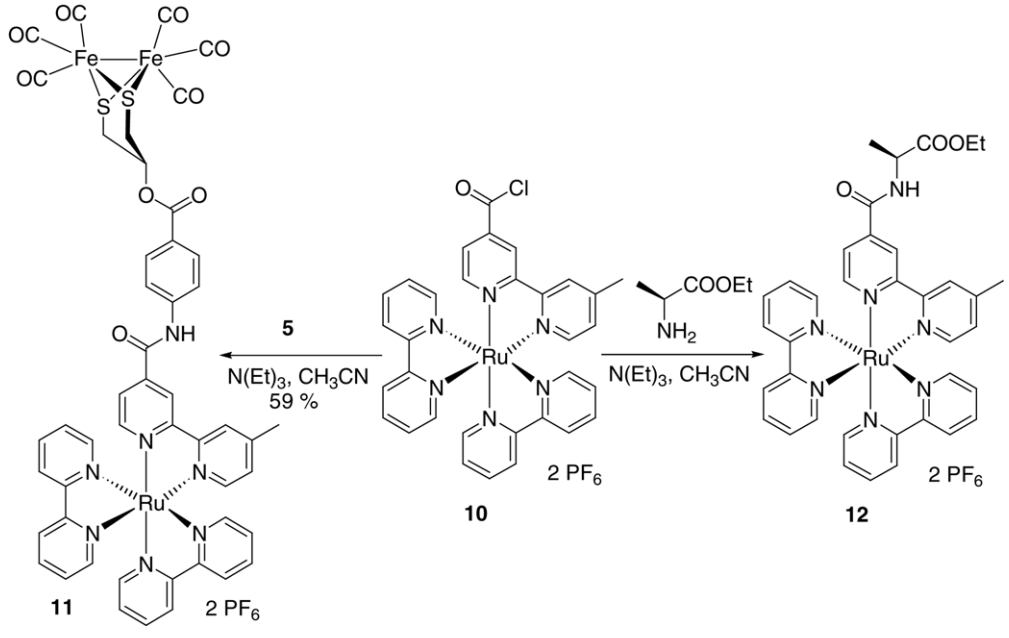

Scheme 4. Synthesis of Ru–Fe_2 dyad **11** and reference complex **12**.

amine as well as on the diiron portion of the complex. Efforts to determine the location of the electron hole in oxidized **8** and **9** by spectroscopic techniques (ESR, UV–vis) were unsuccessful due to the instability of the oxidized species [41]. The irreversible reduction associated with the diiron unit proceeds at a potential somewhat less negative than that of **4**, around -1.55 ± 0.02 V. From these data, it seems that [(μ-ADT)$Fe_2(CO)_6$] complexes are superior as acceptors in electron transfer processes to the all-carbon bridged analogues.

3. Ruthenium–diiron dyads

3.1. Synthesis

Starting from the functionalized diiron complexes **5**, the synthesis of the corresponding dyad **11** proceeded as anticipated. Hence, the acid chloride of [$(bpy)_2$Ru(4-Me-4′-COOH-bipyridine)]$^{2+}$ **10** which is available by heating the latter complex in thionylchloride, reacts smoothly with the amino-equipped **5** to form dyad **11** in good yield (Scheme 4) [42].

Model complex **12** [43] was prepared from **10** and alanine ethylester in a similar procedure and was used for comparison of the photophysical properties of **11**.

The iodo-functionalized diiron complex **8** could be converted to the corresponding dyad by reacting the former complex with 4′-ethynyl-2,2′:6′,2″-terpyridine [44,45] under Sonogashira cross-coupling conditions [46] to afford the diiron complex **13** with an appended terpyridine metal binding site (Scheme 5). In the solid state, the iron carbonyl portion of **13** is stable towards ligand substitution by the polypyridine as unambiguously demonstrated by single crystal X-ray diffraction (Fig. 4). Apart from the ethynylterpyridine fragment, the crystal structure of **13** closely resembles that of **8**. Benefiting from the rigidity of the system, the distance from the nitrogen atom (N) of the central pyridine ring to the two iron cations could be calculated to be 11.892(3) and 13.996(3) Å, respectively.

Solutions of **13** in organic solvents are unstable at room temperature and decompose within minutes upon exposure to light, presumably due to light-induced decarbonylation followed by intermolecular terpyridine complexation. However, as a freshly prepared solution in methanol which is kept in the dark, ligand **13** coordinates readily to the (terpy)Ru fragment, [47] giving rise to the desired trinuclear complex **14**. In contrast to **13**, solutions of **14** are stable and can be stored at ambient atmosphere for weeks. However, over a period of months, dyad **14** decomposes even in the solid state, presumably due to oxidative degradation of the acetylene linker.

In order to have a reference system comparable to **14**, the 4-(*N*-piperidyl)phenylethynyl-terminated [$Ru(terpy)_2$]$^{2+}$ complex **16a** as well as its phenylethynyl-analogue **16b** were synthesized in procedures analogous to that for the preparation of **14**. Hence, iodo-4-(*N*-piperidyl)benzene [48] was reacted with 4′-ethynyl-2,2′:6′,2″-terpyridine [45] to produce the acetylenic ligand **15a** and phenyl acetylene was reacted with 4′-[((trifluoromethyl)sulfonyl)oxy]-2,2′:6′,2″-terpyridine [44,49] to form **15b**. Subsequently, both ligands were separately coordinated to the (terpy)Ru fragment in refluxing ethanol, thereby forming **16a** and **16b** (Scheme 6) [41].

Dyad **14** differs from **11** in many respects, most prominently in that it contains a [$Ru(terpy)_2$]$^{2+}$-type photosensitizer compared to a [$Ru(bpy)_3$]$^{2+}$-type chromophore in **11**. Terpy-based systems offer the advantage that a linear geometry becomes accessible and no isomeric mixtures are obtained when the system is further extended, i.e. by the covalent attachment of an electron donor. However, this strategy also suffers from certain drawbacks as the excited state lifetimes

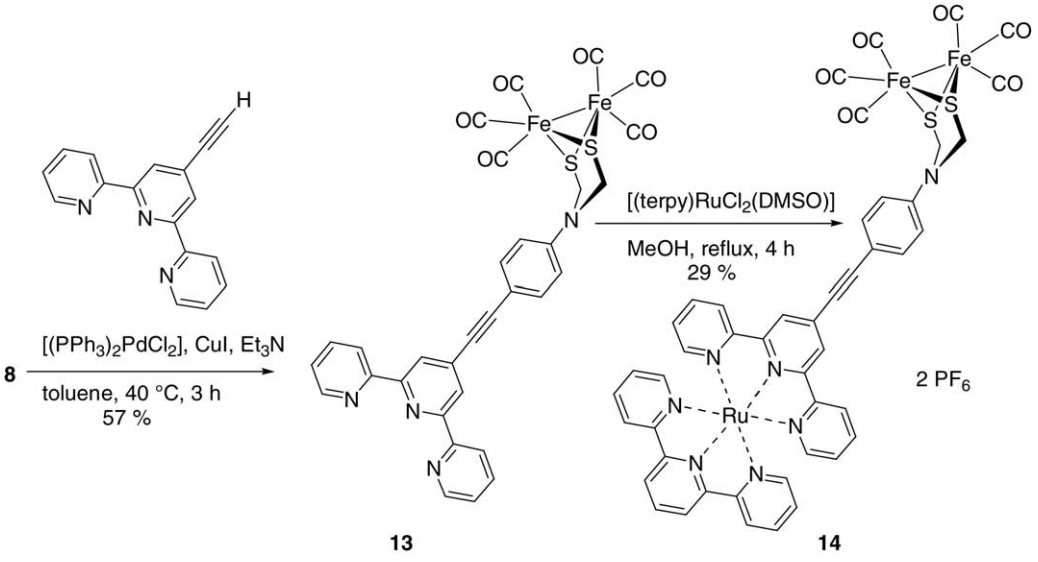

Scheme 5. Synthesis of Ru–Fe_2 dyad **14**.

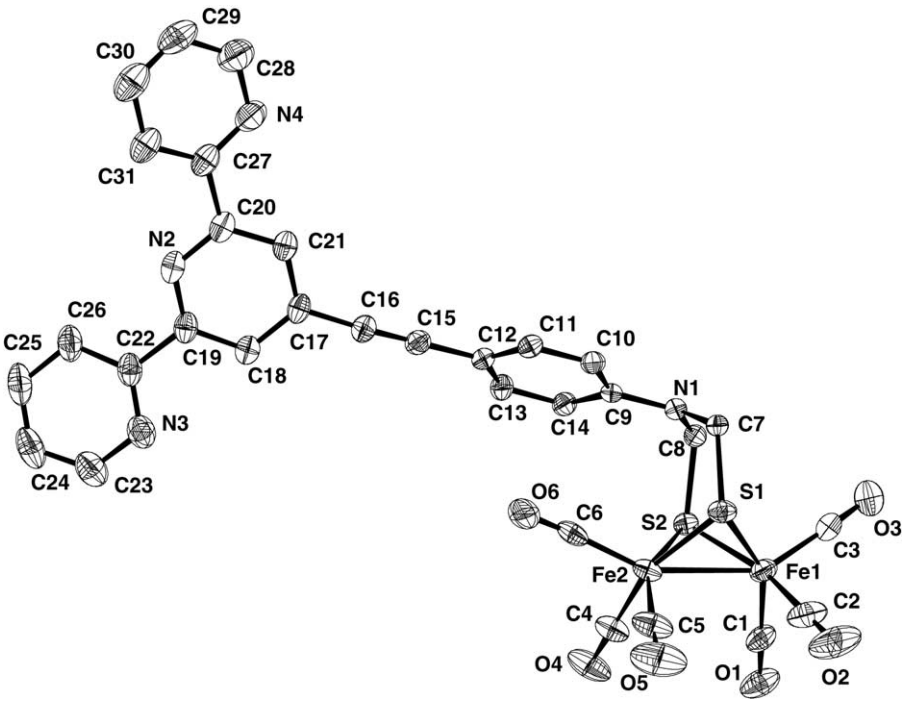

Fig. 4. ORTEP (ellipsoids at 30% probability level) view of terpyridine-equipped [(ADT)$Fe_2(CO)_6$] **13**. Reproduced with permission of the copyright holders from [37].

are generally shorter and the excited state energies lower compared to bpy-based systems. Whereas the linking unit in **11** is flexible which could give rise to several conformers, the rigidity of the phenylacetylene tether in **14** allows precise control over the spatial separation between the ruthenium and diiron moiety. Furthermore, less functional groups in the linker may translate to higher chemical stability, in particular towards nucleophilic attack. Finally, the potential proton reduction site is composed of a diiron hexacarbonyl portion in both dyads, but differs in the nature of the central atom in the dithiolate bridge. The extend to which these different designs influence the properties of the dyads are discussed in the following section.

3.2. Electronic properties

3.2.1. IR spectra

The IR spectrum of dyad **11** (recorded in CH_2Cl_2) features three characteristic peaks between 2075 and 2000 cm^{-1} originating from the carbonyl ligands. In this region, the spectrum of **11** is essentially identical to that of the precursor **4** which lacks the ruthenium tris-bipyridine moiety. Further-

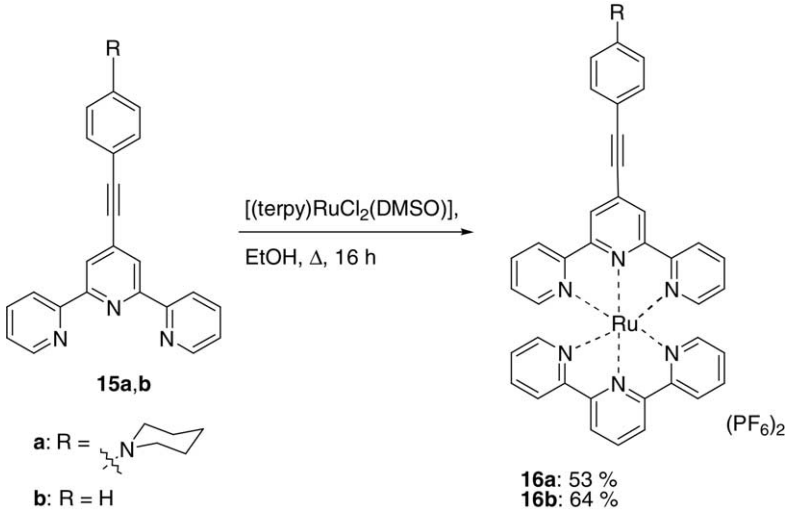

Scheme 6. Synthesis of reference complexes **16a** and **16b**.

more, both spectra are in agreement with that reported for [(μ-PDT)$Fe_2(CO)_6$]. Since an electronic communication between the diiron moiety in **11** and the appended ruthenium photosensitizer would most probably result in changed carbonyl IR frequencies, the absence of such a shift points towards an electronic isolation of the two redox active moieties in the ground state. Similar to the situation in **11**, a comparison between the IR spectra of dyad **14** and those of the related precursors **8** and **13** reveals that they are almost superimposable in the carbonyl region and that no communication between the different units is operating in the ground state.

3.2.2. Electronic absorption spectra

The trinuclear ruthenium–diiron complex **11** displays an electronic absorption spectra typical for $[Ru(bpy)_3]^{2+}$ type of complexes [50]. The strongest absorption in the UV around 290 nm is usually attributed to bpy-centred $\pi \rightarrow \pi^*$ transitions. The longest wavelength absorption around 460 nm is caused by metal-to-ligand charge transfer (MLCT) transitions of the $[Ru(bpy)_3]^{2+}$ moiety [50]. An additional band at 328 nm is visible which correlates well with a transition in the isolated diiron complex **5** at similar energy. The low energy MLCT band overlays the weak absorption from the diiron portion in **11**.

The piperidine-containing terpyridine **15a** features a strong absorption at 362 nm in addition to a band in the far UV. The UV–vis spectrum of ligand **13** exhibits three intense absorptions at 278, 341 and 357 nm, thereby suggesting that it can be regarded as a simple combination of the spectra of **8** and that of the reference ligand **15a** (Fig. 5) [41]. As expected for $[Ru(terpy)_2]^{2+}$ type complexes [50], the absorptions in the UV–vis spectrum of the trinuclear complex **14** are red-shifted compared to those of dyad **11** with strong absorptions at 310 nm and around 500 nm. The latter band overlays the weak, low-energy absorption from the diiron moiety in **14**. The diiron-based transition at 325 nm is visible as a shoulder in the spectrum of **14**.

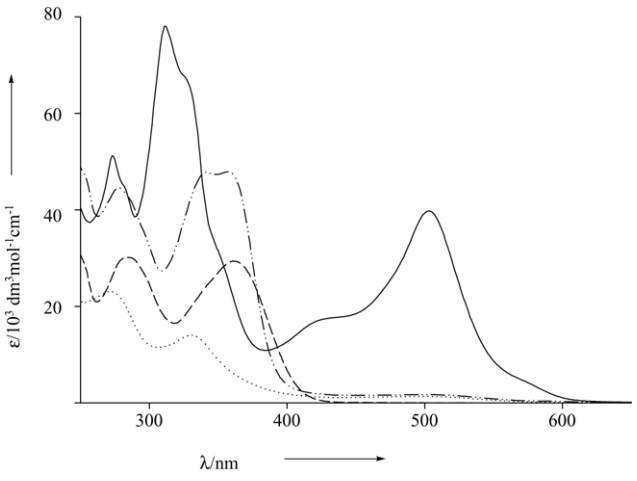

Fig. 5. Electronic absorption spectra of **8** (···), **13** (–·–), **14** (—) and **15a** (– – –), recorded in CH_2Cl_2.

3.2.3. Electrochemistry

The driving force for an electron transfer from the photo-excited ruthenium polypyridyl portion to the diiron site in the dyads can be calculated from the electrochemical data in conjunction with the excited state energies (see emission section below). Hence, a knowledge of the redox properties of the dyads is clearly desired. The cyclic voltammogram of dyad **11** features presumably three overlaying oxidations below 1 V, originating from the irreversible oxidation of the diiron portion, the irreversible oxidation of the amine and the reversible $Ru^{III/II}$ oxidation. On the reductive scan, a poorly resolved reduction is visible around –1.6 V versus $Fc^{+/0}$, besides further irreversible peaks arising from the reduction of the bipyridine ligands coordinated to the ruthenium center.

The Ru(II)/Ru(III) couple in the $[Ru(terpy)_2]^{2+}$ complexes **14**, **16a** and **16b** is observed at 0.93 ± 0.02 V. The irreversible oxidation of the diiron moiety in **14** proceeds at 0.65 V and is thus shifted to higher potentials by 100 mV compared to the oxidations of isolated diiron complexes **8** and **9**. Reduction of **14** at −1.49 V proceeds at a potential slightly less negative than those usually observed for the reduction of the terpyridine ligands and can thus be assigned to the reduction of the diiron portion. The remaining reduction waves for **14** at −1.67 and −1.89 V and around −1.6 and −1.9 V for **16a** and **16b** are typical for $[Ru(terpy)_2]^{2+}$ complexes and arise from the reduction of the terpyridine ligands [50].

3.2.4. Emission data

The driving force for electron transfer from the ruthenium to the diiron site in dyads **11** and **14** can be calculated from the excited state energies and the reduction potentials discussed in the previous section, using the Rehm–Weller equation [51]. With the assumption that the excited state energy of dyad **11** is similar to that of the reference complex **12**, this process can be determined to be endothermic by roughly 400 mV. The emission of dyad **11** follows a double exponential decay function with lifetimes of $\tau_1 = 234$ ns (with an amplitude of circa 20%) and $\tau_2 = 1190$ ns (80%). Compared to the emission of the reference complex **12** which decays single exponentially with a lifetime of 1380 ns, it appears that the emission from **11** is quenched to about 70%. Steady-state emission data show similar results with the emission of **11** being quenched to 60%. The quenching is attributed to energy transfer and the non-exponential behavior to different conformations of the flexible linker. Although the linker appears to be linear in the crystal structure of diiron complex **5**, the tether could bend and place the diiron unit close to the ruthenium chromophore in solutions of **11**.

The excited state energies of complexes **14** and **16a, 16b** were determined from the emission spectra recorded in a solvent glass at 77 K [52–54]. For complexes **14**, **16a** and **16b** the excited state energies were calculated to be 1.89, 1.89 and 1.91 eV, respectively. As an effect of the better electron accepting capacity of the ligands in these complexes, these values are slightly lower than that for $[Ru(terpy)_2]^{2+}$ (2.07 eV) [55]. The driving force for electron transfer from

the ruthenium to the diiron site was calculated as above with the Rehm–Weller equation [51]. Using the reduction potentials from the cyclic voltammetry data and omitting the work term arising from coulombic interactions, the driving force was calculated to be uphill with $\Delta G^0 = 0.59$ eV.

The excited state decay, as determined from the time-resolved emission decay traces, gave lifetimes of 23 ns for **16a**, 13.5 ns for **16b** and 6.5 ns for **14**. The excited state decay is significantly faster in **14** than in **16a** and **16b**. The quenching rate constant k_q can be estimated as $k_q = 1/\tau_{\mathbf{14}} - 1/\tau_{\mathbf{16a}} = 1.1 \times 10^8\ s^{-1}$. Since the electron transfer to the diiron moiety is strongly endothermic, the quenching is not induced by electron transfer but rather by dipole–dipole energy transfer. A calculation of the rate constant using Förster's equation [56] with the orientation factor κ set to 1 and a donor acceptor distance of 8.5 Å gave a value of a similar magnitude as the experimental one. The exact location of the excited state in **14** is somewhat ambiguous but a donor–acceptor distance of 8.5 Å is not unreasonable, considering that the distance between the terpyridine ligand and the diiron center was found to be 12–14 Å in the crystal structure of complex **13**. It appears therefore that Förster energy transfer is a plausible explanation for the quenching in **14** [41].

4. Conclusions

With the preparation of **11** and **14**, the first ruthenium polypyridyl–diiron dyads have been synthesized. However, the redox properties of the ruthenium and diiron components in both dyads are unfavorable for electron transfer, let alone for the reduction of protons to molecular hydrogen. The reduction potential of the excited state of the ruthenium portion (*Ru) is insufficient and the driving force for electron transfer is uphill by circa half a volt in **11** and **14**. Another common feature of both dyads is that energy transfer to the diiron subunit is responsible for a quenching of the ruthenium-based excited state, thereby causing a decrease of the excited state lifetime. The energy transfer quenching is modest and will probably not seriously compete with electron transfer once the redox properties are adjusted to more favorable values. The reduced excited state lifetime particularly in **11** is still sufficiently long to allow electron transfer in the next generation of Ru–Fe_2 complexes. With our experience in electrochemical proton reduction, we believe that protonation of the nitrogen in the ADT bridge in dyads of type **14** can shift the reduction potential of the diiron subunit to more positive values, thereby rendering the electron transfer process thermodynamically more favourable. Alternatively, introduction of different ligands on the diiron core could have a similar effect. Ligands such as cyanides and phosphines have been shown to increase the electron density of the iron–iron bond, thereby facilitating its protonation and decreasing the potential required for the electrochemical production of hydrogen [30,31]. With the inclusion of these structural features in the design of the next generation of ruthenium diiron dyads, we hope to be able to provide sufficient reducing power to drive an electron transfer to a biomimetic model of the iron hydrogenase active site. Efforts in these directions are currently in progress.

Acknowledgements

Financial support for this work was provided by the Swedish Energy Agency, the Knut and Alice Wallenberg Foundation and the Swedish Research Council (VR). The authors wish to acknowledge the numerous collaborators and co-workers who have contributed to this work, especially Dr. Reiner Lomoth and Profs. Leif Hammarström and Stenbjörn Styring at Uppsala University, Sweden.

References

[1] Energy Special Issue 4134, Science 184 (1974).
[2] P. Hoffmann, Tomorrow's Energy: Hydrogen, Fuel Cells, and the Prospect for a Cleaner Planet, MIT Press, Cambridge, Massachusetts, London, England, 2001.
[3] L.O. Williams, An End to Global Warming, Pergamon, Amsterdam, 2002.
[4] M.I. Hoffert, K. Caldeira, A.K. Jain, E.F. Haites, L.D.D. Harvey, S.D. Potter, M.E. Schlesinger, S.H. Schneider, R.G. Watts, T.M.L. Wigley, D.J. Wuebbles, Nature 395 (1998) 881.
[5] K.K. Rao, R. Cammack, in: R. Cammack, M. Frey, R. Robson (Eds.), Hydrogen as a Fuel, Learning from Nature, Taylor & Francis, London, New York, 2001.
[6] E. Amouyal, Sol. Energy Mater. Sol. Cells 38 (1995) 249.
[7] A. Harriman, M.A. West (Eds.), Photogeneration of Hydrogen, Academic Press, New York, 1982.
[8] J.-M. Lehn, J.-P. Sauvage, Nouv. J. Chim 1 (1977) 449.
[9] K. Kalyanasundaram, J. Kiwi, M. Grätzes, Helv. Chim. Acta 61 (1978) 2720.
[10] A. Moradpour, E. Amouyal, P. Keller, H. Kagan, Nouv. J. Chim. 2 (1978) 547.
[11] Z. Zou, J. Ye, K. Sayama, H. Arakawa, Nature 414 (2001) 625.
[12] S.U.M. Khan, M. Al-Shahry, W.B. Ingler Jr., Science 297 (2002) 2243.
[13] J.W. Peters, Curr. Opin. Struct. Biol. 9 (1999) 670.
[14] R. Cammack, Nature 397 (1999) 214.
[15] F.A. Armstrong, Curr. Opin. Chem. Biol. 8 (2004) 133.
[16] M. Frey, Chem. Bio. Chem. 3 (2002) 152.
[17] J.W. Peters, W.N. Lanzilotta, B.J. Lemon, L.C. Seefeldt, Science 282 (1998) 1853.
[18] Y. Nicolet, C. Piras, P. Legrand, E.C. Hatchikian, J.C. Fontecilla-Camps, Structure 7 (1999) 13.
[19] H.-J. Fan, M.B. Hall, J. Am. Chem. Soc. 123 (2001) 3828.
[20] Y. Nicolet, A.L. de Lacey, X. Vernede, V.M. Fernandez, E.C. Hatchikian, J.C. Fontecilla-Camps, J. Am. Chem. Soc. 123 (2001) 1596.
[21] A. Winter, L. Zsolnai, G. Huttner, Z. Naturforsch. 37b (1982) 1430.
[22] J.D. Lawrence, T.B. Rauchfuss, S.R. Wilson, Inorg. Chem. 41 (2002) 6193.
[23] E.J. Lyon, I.P. Georgakaki, J.H. Reibenspies, M.Y. Darensbourg, Angew. Chem. Int. Ed. 38 (1999) 3178.
[24] E.J. Lyon, I.P. Georgakaki, J.H. Reibenspies, M.Y. Darensbourg, J. Am. Chem. Soc. 123 (2001) 3268.

[25] M. Razavet, S.C. Davies, D.L. Hughes, C.J. Pickett, Chem. Commun. (2001) 847.
[26] M. Razavet, S.J. Borg, S.J. George, S.P. Best, S.A. Fairhurst, C.J. Pickett, Chem. Commun. (2002) 700.
[27] S.J. George, Z. Cui, M. Razavet, C.J. Pickett, Chem. Eur. J. 8 (2002) 4037.
[28] X. Zhao, I.P. Georgakaki, M.L. Miller, R. Mejia-Rodriguez, C.-Y. Chiang, M.Y. Darensbourg, Inorg. Chem. 41 (2002) 3917.
[29] D.J. Evans, C.J. Pickett, Chem. Soc. Rev. 32 (2003) 268.
[30] F. Gloaguen, J.D. Lawrence, T.B. Rauchfuss, J. Am. Chem. Soc. 123 (2001) 9476.
[31] F. Gloaguen, J.D. Lawrence, T.B. Rauchfuss, M. Benard, M.-M. Rohmer, Inorg. Chem. 41 (2002) 6573.
[32] S. Ott, M. Kritikos, B. Åkermark, L. Sun, R. Lomoth, Angew. Chem. Int. Ed. (2004) 1006.
[33] L. Sun, L. Hammarström, B. Åkermark, S. Styring, Chem. Soc. Rev. 30 (2001) 36.
[34] L. Hammarström, Curr. Opin. Chem. Biol. 7 (2003) 666.
[35] S. Salyi, M. Kritikos, B. Åkermark, L. Sun, Chem. Eur. J. 9 (2003) 557.
[36] C. He, M. Wang, X. Zhang, Z. Wang, C. Chen, J. Liu, X. Peng, B. Åkermark, L. Sun, Angew. Chem. Int. Ed. (2004) 3571.
[37] S. Ott, M. Kritikos, B. Åkermark, L. Sun, Angew. Chem. Int. Ed. (2003) 3285.
[38] J.D. Lawrence, H. Li, T.B. Rauchfuss, Chem. Commun. (2001) 1482.
[39] F. Gloaguen, J.D. Lawrence, M. Schmidt, S.R. Wilson, T.B. Rauchfuss, J. Am. Chem. Soc. 123 (2001) 12518.
[40] All reduction potentials reported herein are cathodic peak potentials and are calibrated versus $Fc^{+/0}$.
[41] S. Ott, M. Borgström, M. Kritikos, R. Lomoth, J. Bergquist, B. Åkermark, L. Hammarström, L. Sun, Inorg. Chem. 43 (2004) 4683.
[42] H. Wolpher, M. Borgström, L. Hammarström, J. Bergquist, V. Sundström, S. Styring, L. Sun, B. Åkermark, Inorg. Chem. Commun. (2003) 989.
[43] A. Magnusson, H. Berglund, P. Korall, L. Hammarström, B. Åkermark, S. Styring, L. Sun, J. Am. Chem. Soc. 119 (1997) 10720.
[44] K.T. Potts, D. Konwar, J. Org. Chem. 56 (1991) 4815.
[45] V. Grosshenny, F.M. Romero, R. Ziessel, J. Org. Chem. 62 (1997) 1491.
[46] K. Sonogashira, Y. Tohda, N. Hagihara, Tetrahedron Lett. (1975) 4467.
[47] T. Norrby, A. Börje, B. Åkermark, L. Hammarström, J. Alsins, K. Lashgari, R. Norrestam, J. Mårtensson, G. Stenhagen, Inorg. Chem. 36 (1997) 5850.
[48] F. Effenberger, W. Agster, P. Fischer, K.H. Jogun, J.J. Stezowski, E. Daltrozzo, G. Kollmannsberger-von Nell, J. Org. Chem. 48 (1983) 4649.
[49] E.C. Constable, M.D. Ward, J. Chem. Soc., Dalton Trans. (1990) 1405.
[50] J.-P. Sauvage, J.-P. Collin, J.-C. Chambron, S. Guillerez, C. Coudret, V. Balzani, F. Barigelletti, L. De Cola, L. Flamigni, Chem. Rev. 94 (1994) 993–1019.
[51] D. Rehm, A. Weller, Isr. J. Chem. 8 (1970) 259.
[52] L. Hammarström, F. Barigelletti, L. Flamigni, M.T. Indelli, N. Armaroli, G. Calogero, M. Guardigli, A. Sour, J.-P. Collin, J.-P. Sauvage, J. Phys. Chem. A 101 (1997) 9061.
[53] J.V. Caspar, T.J. Meyer, Inorg. Chem. 22 (1983) 2444.
[54] J. Treadway, B. Loeb, R. Lopez, P.A. Anderson, F.R. Keene, T.J. Meyer, Inorg. Chem. 35 (1996) 2242.
[55] M. Maestri, N. Armaroli, V. Balzani, E.C. Constable, A.M.W. Cargill Thompson, Inorg. Chem. 34 (1995) 2759.
[56] T. Förster, Discuss. Faraday Soc. (1959) 7.